TDMA Slot Allocation for UAV Formations: Minimum Superframe Lengths for Two-Dimensional Equidistant Deployments

Amelia Samandari
Department of Computer Science
University of Canterbury
Christchurch, New Zealand
amelia.samandari@pg.canterbury.ac.nz

Andreas Willig
Department of Computer Science
University of Canterbury
Christchurch, New Zealand
andreas.willig@canterbury.ac.nz

***Abstract*—This paper looks at the case of mitigating collisions between UAVs in a formation through the use of safety beacons to relay information about UAVs that are at risk of collision due to their geographic proximity to one another. The UAVs send these safety beacons using time division multiple access (TDMA). With TDMA, UAVs can achieve collision-free transmission, thereby reducing the uncertainty of the UAVs in the formation receiving the necessary safety information. In this paper, we provide a system model for a specific regular deployment and a spatial reuse scheme for allocating UAVs to a TDMA slot that operates as follows: the regular, two-dimensional UAV deployment is partitioned into a hexagonal tiling, where all UAVs in the same tile are allocated to different TDMA slots and all UAVs in the same position in their respective tiles are allocated to the same TDMA slot. Through spatial reuse of TDMA slots, our scheme can support large formations with a bounded transmission period (i.e. a bounded superframe length). We also ascertain a safety margin factor for the transmit power that can be applied to moderate the effects of interference from multiple UAVs transmitting in the same time slot.**

***Index Terms*—unmanned aerial vehicle (UAV), drone, multi-UAV systems, UAV formations, medium access control (MAC), time division multiple access (TDMA), spatial reuse**

I. Introduction

There is an abundance of research on single-UAV (unmanned aerial vehicles) or drone architectures and applications. Such research often focuses on the integration of drone into an existing application (e.g. aerial imaging, infrastructure monitoring, telecommunications), the modification of the drone for improved or autonomous navigation and control, or on ground-air communications [1]–[4].

Recently, there has been increased interest in multi-UAV systems, in which a number of UAVs collaborate to achieve a common goal, supported by a wireless network allowing close collaboration and coordination between drones. These include deployment of a multi-UAV system to assist search and rescue [5], provide communications channels in the aftermath of disaster scenarios [3] or support wildlife tracking [6].

In this context, we can roughly distinguish between UAV swarms and UAV formations. In a swarm, the underlying wireless network is fully connected but there is no prescription as to where individual drones have to be relative to other swarm members and their neighbourhood relations can change dynamically and in an unplanned way. In contrast, in a drone formation, it is possible to tell at any given time where each drone should be. A special case of a drone formation are rigid formations, in which the relative positions of drones don't change.

In any flying drone network, drones need to communicate frequently with their neighbours, for purposes of collision avoidance and for command and control purposes. We refer to these frequent transmissions as **beacons**. In a highly dynamic topology like in a general drone swarm, the underlying network normally benefits from a quite flexible channel access method like for example CSMA-based protocols, due to the absence of any control traffic and other overheads for distributed resource allocation. In the case of rigid formations, however, it becomes possible to employ TDMA-type MAC protocols, as the initial overhead for slot allocation amortizes in the long run, collisions can be avoided, and it becomes possible to give time and data rate guarantees to drones.

A TDMA protocol generally partitions time into contiguous so-called superframes, which in turn are partitioned into time slots. In a multi-hop network, a particular time slot is allocated to a subset of drones, with this subset being chosen such that their mutual distance is large enough to keep the resulting interference at manageable levels. Any valid allocation of time slots to drones makes sure that every drone gets a time slot in which it can transmit a beacon to its local neighbourhood undisturbed by interference, so that the neighbours can keep track of the drone's position, speed and heading. In this context, our fundamental interest is in determining, for a given rigid drone formation, the smallest possible superframe duration, and therefore the smallest possible period for periodic beacon transmissions. The superframe period determines the amount of uncertainty one drone has about the positions of neighboured drones.

This problem is difficult to answer for a general rigid deployment of drones. In this paper, we consider a special case, in which the drone deployment is two-dimensional and

drones are arranged such that they have an equal distance to all of their immediate neighbours. The allocation of TDMA slots is made in such a way that we partition the deployment into hexagonal tiles of a given "radius", and the superframe size is chosen such that each drone in one such **allocation tile** gets a separate time slot – hence, the superframe size is the same as the number of drones in an allocation tile. Drones in different allocation tiles but with the same relative position within their respective allocation tiles will use the same time slot, enabling spatial reuse.

A key requirement in the choice of an allocation tile is that each drone can transmit its beacons to neighboured drones within the so-called **safety radius** such that any receiver within the safety radius experiences interference levels low enough to ensure reliable reception of beacons. In this paper, interference is restricted to come from other drones in different allocation tiles, we do not consider external interference.

In this paper we present a system model and numerical results for the minimum required superframe size for varying sizes of the drone formation and allocation tile sizes. The main interest in our results lies in providing a baseline against which other MAC protocols aiming to provide reliable periodic beaconing to all neighbours within the safety radius can be compared. Due to our specific assumptions of aligning TDMA superframes with hexagonal allocation tiles, we cannot strictly claim that the resulting allocations are truly optimal, but we hypothesize that in the limit of large formation and allocation tile sizes they are not far away from the optimum superframe size, and that MAC protocols based, for example, on CSMA will not be able to guarantee better reliability to receivers within the safety distance.

The remaining paper is structured as follows: In the next Section II we briefly survey related work. Following this, in Section III we provide our system model, explaining the drone deployment, channel model and protocols, and transmit power and interference assumptions. In Section IV we present a range of numerical results. We conclude the paper in Section V with an outlook on future work.

II. Related Work

In recent years, research has discussed the mass adoption of UAVs for a myriad of practical applications [7]. These applications range from surveillance, including environmental and industrial monitoring [8], to transportation [9], aid in disaster relief efforts [10], [11], aerial photography [12]–[14] and support of agricultural, horticulture, and dairy practices [15]–[17].

For example, in the case of industrial monitoring, UAVs provide a safe alternative to human monitoring and routine testing to prevent catastrophic failures. In addition, it can be impractical, highly costly, or completely infeasible to deploy a human inspector when a high level of regularity is required for thorough monitoring. Some examples of such industrial monitoring cases include wind turbines, high-rise buildings, bridges, oil flare stacks, and power transmission towers.

There is also a greater interest in the adoption of multi-UAV systems for these practical applications. The increased interest in multi-UAV systems is in large part due to the flexibility, mobility, adaptability, and effortless deployment of these systems. They can be of benefit in diverse scenarios that span social, economic, and environmental spheres across countless industries. Multi-UAV systems can perform many tasks faster [18], [19] and/or more completely [6] than humans. Furthermore, depending on the method employed to control a multi-UAV system, a single human controller can direct many UAVs, thus making the use of UAVs far more practical and resource-efficient.

A. Spatial Reuse

Prior research has considered spatial reuse in the case of multi-hop communication in wireless mesh networks [20]. The issues faced in the case of effective TDMA-based communication in a UAV formation, which motivate spatial reuse, are similar to those in wireless mesh networks. Namely, nodes utilize the same broadcast medium and nodes have a limited transmission range. As a result, resource allocation and scheduling of channel access are critical for collision-free transmission.

Furthermore, when transmissions are propagated on a multi-hop basis (as in wireless mesh networks) or in cases where transmissions are only relevant for a limited area (as in safety beacons for a UAV formation), it is possible to leverage the limited transmission range of a node to allow for multiple nodes to transmit simultaneously without collision [20]. Naturally, this necessitates an appropriate hop distance between transmitters, to account for hidden terminals, as well as the configuration of the transmission power used. This is done to prevent collisions, mitigate interference and achieve successful packet reception.

B. UAV Communication Channel Modeling

The unique characteristics of communications in multi-UAV systems, which are divergent from those found in traditional wireless communications, are the existence of two distinct communication channels (air-ground and air-air), non-stationary channels that experience spatial and temporal variation, and the effects of shadowing from the UAVs themselves. Our work focuses specifically on using the air-air communication channel to distribute safety information between UAVs in the formation.

Research has shown that using commercially available 802.11 radios for UAV channel characterization is advantageous as it is a low-cost, low-power option that can be flexibly integrated with UAVs [21]. Constraints come in the form of their limited communication range, narrow-band frequency, and their susceptibility to interference and noise. Because our work considers spatial reuse and parallel transmissions, the constraint of a limited communication range facilitates the desired ability to have multiple concurrent transmissions.

III. System Model

In this section we introduce our system model.

A. UAV Formation Deployment

We consider a two-dimensional drone formation deployment where all drones have the same altitude, high enough to eliminate reflections or interference from the ground. The drones are arranged in a hexagonal pattern, where each drone has up to six immediate neighbors, and it has the same distance r to each of those. We fix one particular drone in our formation, which we refer to as the **center drone**, and around which all other drones are arranged in complete, concentric "hexagonal rings".

We describe the drone positions by assigning two-dimensional coordinates to them (the altitude information is suppressed). We define two two-dimensional vectors:

$$\mathbf{e}_1 = \begin{pmatrix} r \\ 0 \end{pmatrix} \quad , \quad \mathbf{e}_2 = \begin{pmatrix} \frac{r}{2} \\ \frac{r\sqrt{3}}{2} \end{pmatrix}$$

The position of any drone in the formation can be described by a vector $a \cdot \mathbf{e}_1 + b \cdot \mathbf{e}_2$ where $a, b \in \mathbb{Z}$. Hereon, we will refer to a drone by its associated coordinate pair (a, b). The center drone has the coordinates $(0, 0)$ and its immediate neighbors have the coordinates $(1, 0)$,$(-1, 0)$, $(0, 1)$, $(0, -1)$, $(1, -1)$ and $(-1, 1)$. These immediate neighbors of the center drone are said to be in the first tier of the formation. Those drones that are neither the center drone nor in the first tier but which have a first-tier drone as an immediate neighbour, are referred to as second-tier drones, and so on. To generate the coordinates of the drones in tier n, we use the following prescription:

- Corner points: $(n, 0)$, $(-n, 0)$, $(0, n)$, $(0, -n)$, $(n, -n)$, $(-n, n)$
- The points $(x, n - x)$ for $x \in \{1, \ldots, n - 1\}$
- The points $(-x, -(n - x))$ for $x \in \{1, \ldots, n - 1\}$
- The points $(-x, n)$ for $x \in \{1, \ldots, n - 1\}$
- The points $(x, -n)$ for $x \in \{1, \ldots, n - 1\}$
- The points $(n, -x)$ for $x \in \{1, \ldots, n - 1\}$
- The points $(-n, x)$ for $x \in \{1, \ldots, n - 1\}$

Conversely, to determine the tier that a given drone with coordinates (i, j) belongs to, we use the following:

$$\tau(i,j) = \begin{cases} \text{abs}(j) & : \quad i = 0 \\ \text{abs}(i) & : \quad j = 0 \\ \text{abs}(i) + \text{abs}(j) & : \quad \text{sign}(i) = \text{sign}(j) \\ \max\{\text{abs}(i), \text{abs}(j)\} & : \quad \text{otherwise.} \end{cases} \tag{1}$$

We assume that our drone formation consists of completely filled tiers around the center drone.

We operate under TDMA, with a superframe length consisting of a given number of TDMA slots. We partition the drone formation deployment into *allocation tiles*. The central allocation tile is positioned around the center drone at $(0, 0)$ and encompasses an integral number $L \in \mathbb{N}$ of tiers. The central allocation tile, therefore, contains all drones belonging to tiers $[0..L]$ and takes a hexagonal shape. All other allocation tiles have the same shape and size, they are arranged such that they partition the deployment. The distance between the center drone and one of the corner drones of its allocation tile is henceforth referred to as the **allocation tile radius** and it is given by $R = L \cdot r$. The number of TDMA slots in a superframe is equal to the number of drones in an allocation tile, i.e. $1 + 6 \cdot \frac{L(L+1)}{2}$, and the TDMA assignment is such that each drone in the same tile is assigned to a separate time slot. Drones in the same relative position in different allocation tiles are assigned to the same time slot. As such, the size of the allocation tile directly determines the superframe length.

B. Channel Model

We consider a drone formation deployment where all drones fly at an altitude that is high enough to eliminate reflections or interference from the ground. We assume omnidirectional propagation, with no shadowing or reflections by the drones, and therefore also no multi-path propagation. We use the log-distance path loss model with a given path loss coefficient γ and reference-distance path loss PL_0, without fast fading or shadowing. In this model, the received power at a distance $d \geq d_0$ is given by

$$P_r(d) = \frac{P_t}{PL_0} \cdot \left(\frac{d_0}{d}\right)^{\gamma} \tag{2}$$

where P_t is the transmit power and d_0 is the so-called reference or far-field distance, which in this paper we simply assume to be $d_0 = 1$ m. In our setup all drones use the same transmit power.

To keep things simple, we assume that all drones transmit their safety beacons on a common channel that is free from any other kinds of traffic.

C. Protocols

To ensure collision-free flight for drones in the formation, each drone will transmit periodic safety beacons in its allocated TDMA slot. These safety beacons contain the transmitting drone's ID, its current position and velocity vector, amongst other things. We assume their size to be 512 bytes, all included. Furthermore, he size of a TDMA time slot is sufficient to contain a beacon frame plus some safety margin to allow for time synchronization errors. We furthermore assume that all drones have access to time information from GPS, which is highly precise and removes the need for separate time synchronization protocols.

As already mentioned, on the MAC layer all drones use a TDMA protocol – the details of the slot allocation process are outside the scope of this paper and we simply assume that the slot allocation has already been performed. On the physical layer, we assume a WiFi transceiver operating on a 20 MHz channel in the 2.4 GHz ISM band.

D. Transmit Power and Interference

We assume that the deployment consists of an integral number of tiers around the center drone. In such a deployment, the center drone and its neighbors suffer the most from interference. For a TDMA allocation to be feasible, all drones within the given safety radius Δ from the center drone must receive beacons from the center drone with an SINR

exceeding a given threshold Γ. We assume that all drone transceivers experience the same noise power N.

All drones use the same transmit power P_t, which is chosen as follows. For the given path loss model, let P_t' be the transmit power that the center drone must use for a drone at safety distance Δ to receive the transmission with exactly the required SNR Γ in the absence of interference:

$$P_t' = N \cdot \Gamma \cdot PL_0 \cdot \Delta^{\gamma} \tag{3}$$

The transmit power used, P_t, is then chosen as

$$P_t = P_t' \times \epsilon \tag{4}$$

where $\epsilon \geq 1$ provides a safety margin that is used to compensate for interference from drones in neighboured allocation tiles transmitting in the same time slot.

In this paper, we have for reasons of simplicity chosen to set the safety radius Δ to be equal to the drone neighbour distance r, so that we effectively require a sufficient SINR for all tier-one drones. Due to symmetry, we can focus on one tier-one neighbour. To calculate the interference for such a neighbour while receiving a beacon from the center drone, we need to sum up the interference contributions from all other drones at the center of their respective allocation tiles. This in turn requires us to systematically enumerate their positions.

1) Interferer Positions: To enumerate the interferer positions, we introduce the notion of a **ring** (cf. Figure 1a). The zeroth ring consists of the central allocation tile (i.e. the allocation tile containing the center drone), the first ring contains of all allocation tiles that are neighboured to the center allocation tile, the second ring contains all allocation tiles that are not in the center or first ring but are neighboured to a first-ring allocation tile, and so on.

If the formation overall has K completely filled rings surrounding the center ring, then the overall number of allocation tiles is $M = 1 + 6 \cdot \frac{K(K+1)}{2}$, and consequently the overall number of interferers is $M - 1 = 6 \cdot \frac{K(K+1)}{2}$. The overall number of "rows" (cf. Figure 1a) is $2K+1$. The uppermost row has $K+1$ allocation tiles, the next row has $K+2$ allocation tiles, and so on, until the middle row is reached which contains $2K+1$ allocation tiles. From here onward the number of allocation tiles per row counts down to $K+1$.

Using the (a, b) coordinates introduced in section III-A, in the following equations we give the coordinates $(a_{n,m}, b_{n,m})$ of the interferers. The subscript n indicates the row, with $n = 1$ as the top row and $n = N$ as the bottom row, and the subscript m indicates the position in the row, with $m = 1$ as the leftmost point on the row and $m = M$ as the rightmost point on the row (cf. Figure 1b).

The position of the first transmitter can be given as:

$$a_{1,1} = -((2 \times R) + 1) \times K$$
$$b_{1,1} = R \times K$$

where R is the allocation tile radius introduced in Section III-A and as above K is the number of rings in our deploy-

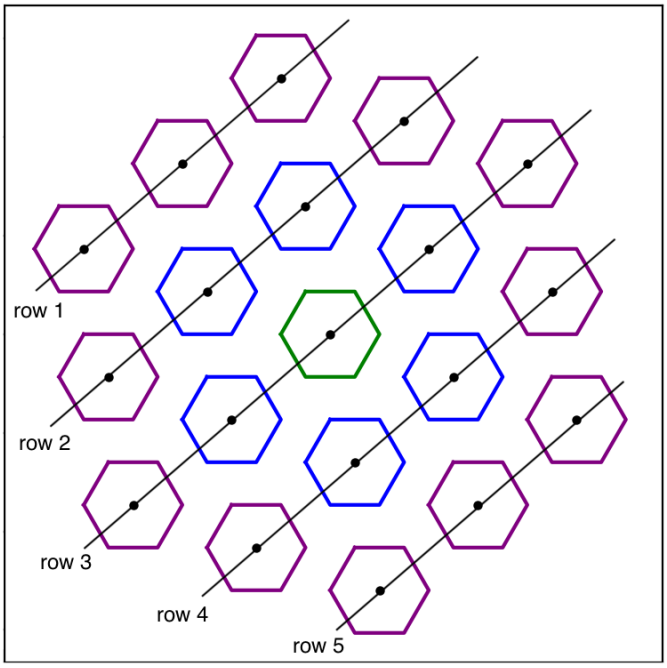

(a) UAV formation with $K = 2$ rings and $N = 5$ rows.

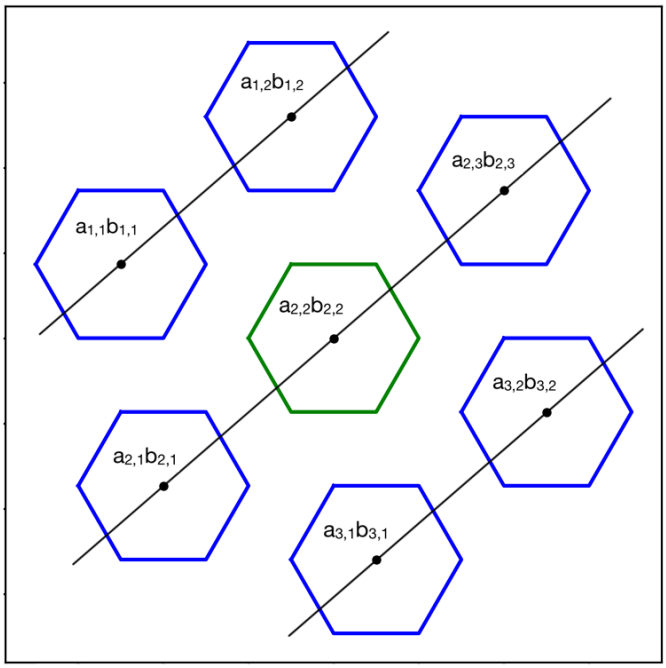

(b) UAV formation with $K = 1$ rings and $N = 3$ rows.

Fig. 1: UAV formation allocation tiles color-coded based on the ring.

ment. The position of the first transmitter on row n can be given as:

$$a_{n,1} = a_{n-1,1} + (1 + R)$$
$$b_{n,1} = b_{n-1,1} - ((2 \times R) + 1)$$

The positions of the transmitters along row n can be given as:

$$a_{n,m} = a_{n,m-1} + R$$
$$b_{n,m} = b_{n,m-1} + (R + 1)$$

2) Feasible Allocations: We consider again the center tile. The center drone transmits a beacon to be successfully received by all drones within the safety radius Δ, in particular by the drone within the safety radius that has the largest distance to the center drone. For simplicity we assume that this drone has just distance Δ to the center drone, so that its received signal power from the center drone transmission is given by

$$R_C = P_r(\Delta) = \frac{P_t' \cdot \epsilon}{PL_0} \cdot \left(\frac{d_0}{\Delta}\right)^{\gamma} \tag{5}$$

(cf. Equations (2) and (4)). The interference observed at the receiving drone coming from one of the interferers is obtained by calculating the distance between the receiving and interfering drone. For the n-th interferer we refer to the resulting power of the interference signal by $R_{I,n}$. Note that $R_{I,n}$ is of the same shape as R_C given in Equation (5), in that it can be written as

$$R_{I,n} = P_r(\Delta_{I,n}) = \frac{P_t' \cdot \epsilon}{PL_0} \cdot \left(\frac{d_0}{\Delta_{I,n}}\right)^{\gamma} \tag{6}$$

where $\Delta_{I,n}$ is the distance between the n-th interferer and the considered receiver node.

Given a safety distance Δ and safety margin ϵ, we regard an allocation tile of size L tiers to be **feasible** when the SINR value exceeds a given threshold Γ, i.e. if

$$\Gamma \geq \frac{R_C}{N + \sum_n R_{I,n}} \tag{7}$$

where N is the noise power. The right-hand side of this inequality, taken as a function of the margin ϵ, is of the form $\frac{\epsilon \cdot C_1}{N + \epsilon \cdot C_2}$ for positive constants C_1 , C_2 and N, which is bounded and strictly increasing for increasing ϵ, i.e. converges to a fixed value, referred to *asymptotic SINR* and denoted by S_a. If $S_a < \Gamma$ then the allocation tile size is infeasible for all choices of ϵ.

The allocation tile size L should always be at least as large as Δ to ensure that all drones within the safety distance are placed in the same allocation tile. Furthermore, the relationship between Δ and the distance between drones in the formation deployment, the aforementioned neighbor distance r, should be such that $r \leq \Delta$.

Parameter	Value	Comment
Protocol and channel parameters		
λ	0.125 m	Wavelength
N	-101 dBm	Total noise power
γ	2	Path loss exponent
PL_0	40 dB	Path loss at reference distance
	512 B	Packet size
Γ	15 dB	Required SINR
Deployment parameters		
r	10 m	Neighbour distance
Δ	10 m	Safety distance

TABLE I: The parameters used, based on transmission over 2.4 GHz WiFi.

E. Key Question

According to our system model, we describe a particular allocation and deployment with the following parameters:

- The deployment size of M tiers, with $M \in \mathbb{N}$, resulting in a total number of $1 + 6 \cdot \frac{M(M+1)}{2}$ drones.
- The neighbour distance r in meters.
- The safety radius Δ in meters.
- The allocation tile size of L tiers, with $L \in \mathbb{N}$. Recalling the notion of rings introduced before, we assume that the deployment size M is chosen such that all rings are complete.
- The transmit power safety margin ϵ.

Given this background, key question addressed in this paper is: For a given M (or alternatively; number of rings $rings$) and r, what is the smallest L and what is the resulting choice of ϵ that leads to a feasible allocation?

IV. Results

In this section we present results for the minimum feasible allocation tile size and sensible choices of ϵ. The results have been obtained numerically. We first describe the settings of relevant system parameters, and then discuss our findings.

A. Parameter Settings

We consider that the drones in the formation are transmitting over a 20 MHz wide channel in the 2.4 GHz range. Transmissions have a wavelength of $\lambda = 0.125$ m and suffer from thermal noise, resulting in a total noise power $N = -101$ dBm. The path loss exponent is $\gamma = 2$ and the path loss at the reference distance is $PL_0 = 40$ dB. Successful transmissions have a minimum required SINR of $\Gamma = 15$ dB. We fix a neighbor distance of $r = 10$m between drones in the formation. The safety radius Δ is also set to 10m. The resulting P_t' (cf. Equation (3)) then becomes -26 dBm. The parameters used can be found in Table I.

B. Choice of ϵ

To determine the setting for the safety margin ϵ, we considered the worst-case SINR for a number of formation settings (e.g. a fixed allocation tile size and formation size).

Formations of size $rings \in \{1, \ldots, 5, 10\}$ and allocation tiles of size $L \in \{1, \ldots, 10\}$ were considered. Select results are shown in Figure 2.

As expected, the results are asymptotic for varying safety margin ϵ for all considered allocation tile sizes and ring numbers. In particular, choosing $\epsilon = 20$ gives a sufficiently good approximation of the asymptotic worst-case SINR values in all considered cases. This is the setting we will adopt for the remaining paper.

Furthermore, the results show that for smaller allocation tile sizes L the worst-case SINR values are significantly worse than for larger L, which can be explained by the fact that for larger L the interference observed at the safety radius becomes smaller as the distance of the interferers grows. For $L = 10$ the only feasible allocations are for one and two rings, when adopting a SINR requirement of $\Gamma = 15$ dB. Note that the gap sizes in worst-case SNR when adding additional rings appear to be almost constant for different values of L.

C. Worst-Case SINR vs. Formation and Allocation Tile Size

To establish the worst SINR that is experienced by a receiving drone in a formation as the allocation tile size increases, we consider a formation of fixed size and increase the allocation tile size $L \in \{1, 2, \ldots, 20\}$. We carry this out for formations of size $rings \in \{1, 2, \ldots, 10, 20\}$. As seen in Figure 3, as the number of rings increases (and hence the number of interfering drones increases), the worst-case SINR decreases.

At the same time, with larger allocation tile sizes, we can increase the worst-case SINR significantly while maintaining the same number of interfering drones. The most significant reduction in worst-case SINR can be observed between the smallest formation size (1 ring) and the next largest formation size (2 rings). The interferers in ring 2 are close enough to the receiver to generate significant interference, whereas the positions of additional interferers in higher rings (3 and higher), by nature of their further distance from the receiver, do not generate as much interference.

D. Allocation Tile Sizes

We now consider the minimum feasible allocation tile size L in tiers for varying number of rings (and therefore varying overall deployment size). Note that the allocation tile size, or more precisely the number of nodes in an allocation tile given by $1 + 6 \cdot \frac{L(L+1)}{2}$, is exactly the same as the required superframe size. Instead of operating with a single target SNR for the worst-case receiver, in this set of results we consider different SNR targets, which we represent as different target packet error rates ($\{1\,\%, 5\,\%, 10\,\%\}$), which is often of higher practical relevance in applications. We consider packets of 512 B size.

In Figure 4 we show for varying number of rings in the system the minimum allocation tile size as a number of tiers that is needed to achieve the indicated packet error rate, and in Figure 5 these results are translated into the corresponding superframe length.

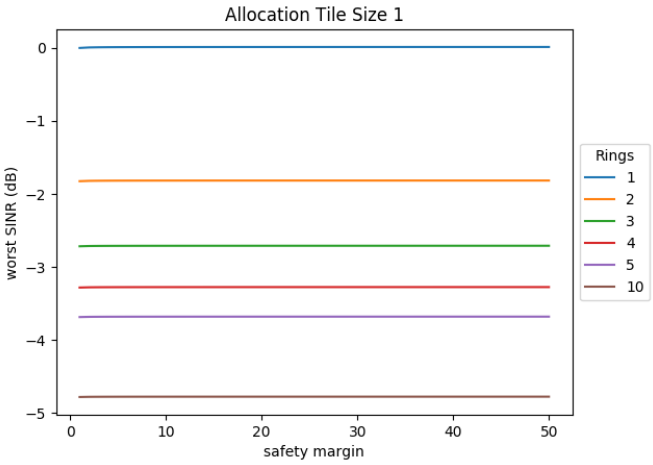

(a) When $L = 1$

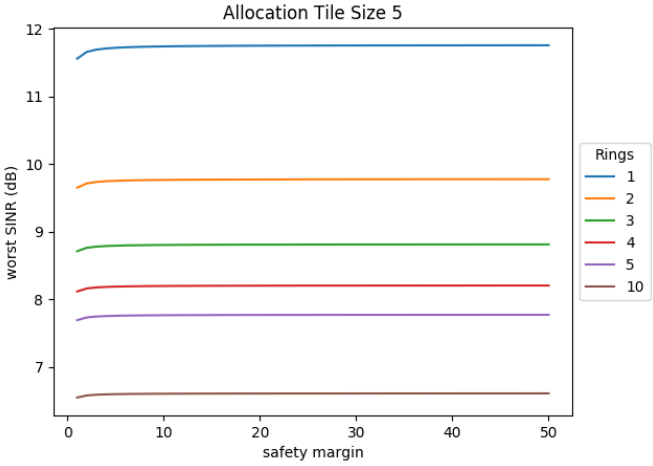

(b) When $L = 5$

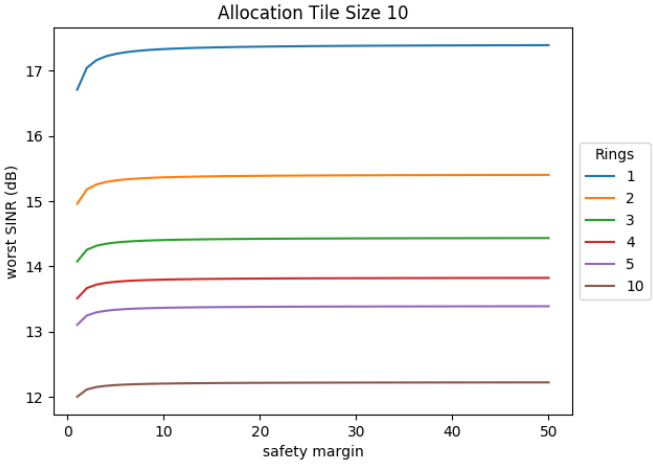

(c) When $L = 10$

Fig. 2: The worst SINR experienced at different allocation tile sizes as the safety margin ϵ increases.

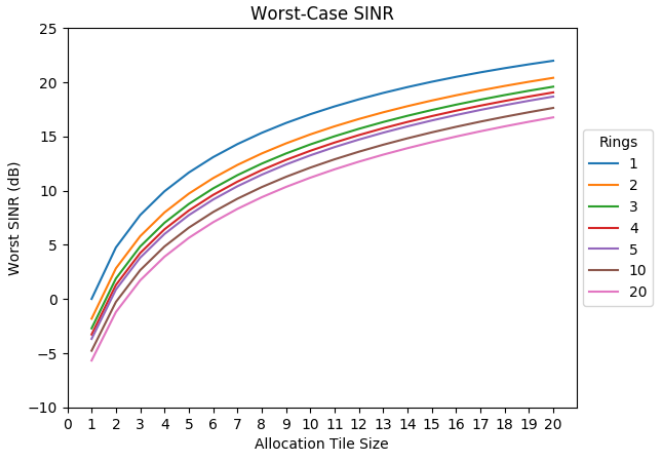

Fig. 3: Worst-case SINR experienced at varying deployment sizes as the allocation tile size increases.

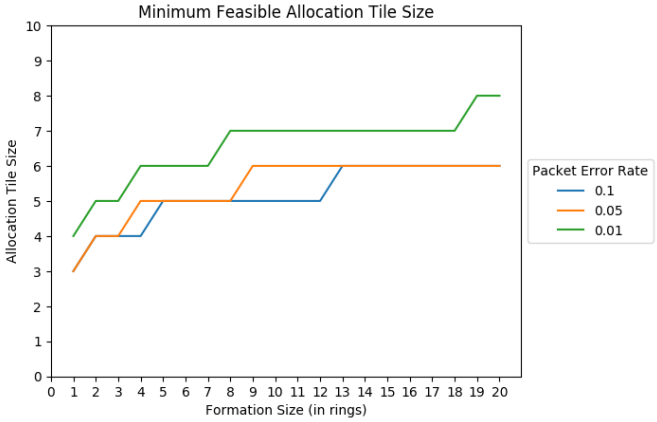

Fig. 4: Minimum feasible allocation tile size to achieve varying packet error rates as the deployment size increases.

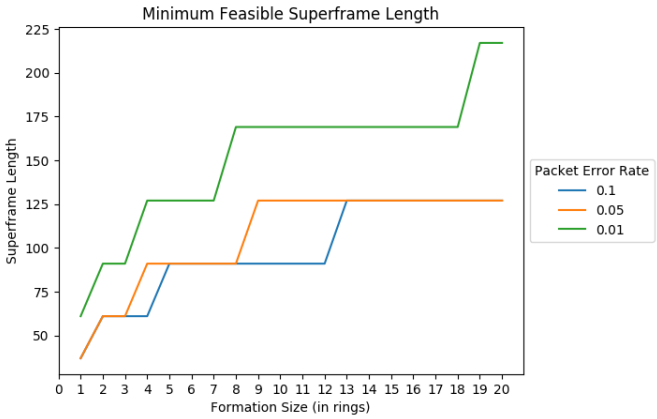

Fig. 5: Minimum superframe length necessary to support the given formation size at each packet error rate.

It can be observed that increasing the number of rings in the formation increases the allocation tile size, though the steps become more widely spaced as $rings$ increases. As previously observed, for fixed safety distance Δ increasing the number L of tiers in an allocation tile leads to larger distances between the worst-case receiver and the interferers. It can furthermore be observed that more relaxed packet error rate targets lead to lead to smaller required allocation tile sizes and therefore smaller superframes.

V. Conclusions

This paper addressed the issue of mitigating collisions between drones in a formation through the use of safety messages that are communicated using a TDMA scheme. We achieve this using a tiling spatial reuse scheme so the necessary superframe length does not increase at the same rate as the formation. We also presented a system model and TDMA allocation scheme for regular, two-dimensional formation deployments that can be partitioned into a hexagonal tiling.

A drone formation can achieve higher network utilization when multiple drones can transmit in the same time slot. Our work determines, based on the number of drones transmitting in the same time slot, the minimum separation between drones that are transmitting concurrently. We also identify a safety margin that can be applied to the base transmit power to moderate the interference generated by other drones transmitting in the same time slot. Given a formation setting (consisting of the number of transmitters and allocation tile size) we ascertain the superframe size that can be supported.

References

[1] Hafiz Suliman Munawar, Fahim Ullah, Siddra Qayyum, and Amirhossein Heravi. Application of deep learning on uav-based aerial images for flood detection. *Smart Cities*, 4(3):1220–1242, 2021.

[2] Najib Metni and Tarek Hamel. A uav for bridge inspection: Visual servoing control law with orientation limits. *Automation in construction*, 17(1):3–10, 2007.

[3] Jesús Sánchez-García, JM García-Campos, Mario Arzamendia, DG Reina, SL Toral, and D Gregor. A survey on unmanned aerial and aquatic vehicle multi-hop networks: Wireless communications, evaluation tools and applications. *Computer Communications*, 119:43–65, 2018.

[4] Mario Arturo Ruiz Estrada and Abrahim Ndoma. The uses of unmanned aerial vehicles–uav's-(or drones) in social logistic: Natural disasters response and humanitarian relief aid. *Procedia Computer Science*, 149:375–383, 2019.

[5] Tullio Joseph Tanzi, Madhu Chandra, Jean Isnard, Daniel Camara, Olivier Sebastien, and Fanilo Harivelo. Towards" drone-borne" disaster management: future application scenarios. In *XXIII ISPRS Congress, Commission VIII (Volume III-8)*, volume 3, pages 181–189. Copernicus GmbH, 2016.

[6] Haluk Bayram, Nikolaos Stefas, Kazim Selim Engin, and Volkan Isler. Tracking wildlife with multiple uavs: System design, safety and field experiments. In *2017 International symposium on multi-robot and multi-agent systems (MRS)*, pages 97–103. IEEE, 2017.

[7] Reza Shakeri, Mohammed Ali Al-Garadi, Ahmed Badawy, Amr Mohamed, Tamer Khattab, Abdulla Khalid Al-Ali, Khaled A Harras, and Mohsen Guizani. Design challenges of multi-uav systems in cyber-physical applications: A comprehensive survey and future directions. *IEEE Communications Surveys & Tutorials*, 21(4):3340–3385, 2019.

[8] Marouane Salhaoui, Antonio Guerrero-González, Mounir Arioua, Francisco J Ortiz, Ahmed El Oualkadi, and Carlos Luis Torregrosa. Smart industrial iot monitoring and control system based on uav and cloud computing applied to a concrete plant. *Sensors*, 19(15):3316, 2019.

[9] Jacek Grzybowski, Karol Latos, and Roman Czyba. Low-cost autonomous uav-based solutions to package delivery logistics. In *Advanced, Contemporary Control*, pages 500–507. Springer, 2020.

[10] Long D Nguyen, Khoi K Nguyen, Ayse Kortun, and Trung Q Duong. Real-time deployment and resource allocation for distributed uav systems in disaster relief. In *2019 IEEE 20th International Workshop on Signal Processing Advances in Wireless Communications (SPAWC)*, pages 1–5. IEEE, 2019.

[11] Christopher Gomez and Heather Purdie. Uav-based photogrammetry and geocomputing for hazards and disaster risk monitoring–a review. *Geoenvironmental Disasters*, 3(1):1–11, 2016.

[12] Arko Lucieer, Darren Turner, Diana H King, and Sharon A Robinson. Using an unmanned aerial vehicle (uav) to capture micro-topography of antarctic moss beds. *International journal of applied earth observation and geoinformation*, 27:53–62, 2014.

[13] Ying-cheng Li, Dong-mei Ye, Xiao-bo Ding, Chang-sheng Teng, Guang-hui Wang, and Tuan-hao Li. Uav aerial photography technology in island topographic mapping. In *2011 International Symposium on Image and Data Fusion*, pages 1–4. IEEE, 2011.

[14] Bin Jiang, Jiachen Yang, and Houbing Song. Protecting privacy from aerial photography: State of the art, opportunities, and challenges. In *IEEE INFOCOM 2020-IEEE Conference on Computer Communications Workshops (INFOCOM WKSHPS)*, pages 799–804. IEEE, 2020.

[15] David Gómez-Candón, AI De Castro, and Francisca López-Granados. Assessing the accuracy of mosaics from unmanned aerial vehicle (uav) imagery for precision agriculture purposes in wheat. *Precision Agriculture*, 15(1):44–56, 2014.

[16] Paulina Lyubenova Raeva, Jaroslav Šedina, and Adam Dlesk. Monitoring of crop fields using multispectral and thermal imagery from uav. *European Journal of Remote Sensing*, 52(sup1):192–201, 2019.

[17] Bijoy Krishna Handique, Chandan Goswami, Chirag Gupta, S Pandit, S Gogoi, R Jadi, P Jena, G Borah, and PLN Raju. Hierarchical classification for assessment of horticultural crops in mixed cropping pattern using uav-borne multi-spectral sensor. *The International Archives of Photogrammetry, Remote Sensing and Spatial Information Sciences*, 43:67–74, 2020.

[18] Igor Kalyaev, Sergey Kapustyan, Donat Ivanov, Iakov Korovin, Leonid Usachev, and Gerald Schaefer. A novel method for distribution of goals among uavs for oil field monitoring. In *2017 6th International Conference on Informatics, Electronics and Vision & 2017 7th International Symposium in Computational Medical and Health Technology (ICIEV-ISCMHT)*, pages 1–4. IEEE, 2017.

[19] Matthew Silic and Kamran Mohseni. Field deployment of a plume monitoring uav flock. *IEEE Robotics and Automation Letters*, 4(2):769–775, 2019.

[20] Rahul Mangharam and Raj Rajkumar. Max: A maximal transmission concurrency mac for wireless networks with regular structure. In *2006 3rd International Conference on Broadband Communications, Networks and Systems*, pages 1–10. IEEE, 2006.

[21] Aziz Altaf Khuwaja, Yunfei Chen, Nan Zhao, Mohamed-Slim Alouini, and Paul Dobbins. A survey of channel modeling for uav communications. *IEEE Communications Surveys & Tutorials*, 20(4):2804–2821, 2018.